

INFLUENCE OF NATURAL CONVECTION AND THERMAL RADIATION MULTI-COMPONENT TRANSPORT IN MOCVD REACTORS

S. Lowry^A, A. Krishnan^B and I. Clark^C

567-34
039144

The influence of Grashof and Reynolds number in Metal Organic Chemical Vapor (MOCVD) reactors is being investigated under a combined empirical/numerical study. As part of that research, the deposition of Indium Phosphide in an MOCVD reactor is modeled using the computational code CFD-ACE. The model includes the effects of convection, conduction, and radiation as well as multi-component diffusion and multi-step surface/gas phase chemistry. The results of the prediction are compared with experimental data for a commercial reactor and analyzed with respect to the model accuracy.

Keywords: Chemical Vapor Deposition (CVD), MOCVD, Computational Fluid Dynamics (CFD), Indium Phosphide, Radiation, Richardson Number

1. INTRODUCTION

Metalorganic Chemical Vapor Deposition (MOCVD) is a common technique for the growth of III-V and II-VI compound semiconductors and alloys. The uniformity and quality of these materials is tightly coupled to the composition and temperature distribution at the growth interface. As such, the understanding and control of heat and mass transport in MOCVD reactors is critical to the production of high quality materials.

The mechanisms of heat and mass transport during MOCVD are currently being investigated under a joint project between CFD Research Corporation and NASA Langley Research Center (LaRC). The research is a combined numerical/experimental study to investigate the influence of radiation and natural convection in MOCVD systems over a range of Richardson (Gr/Re^2) numbers.

2. NUMERICAL MODEL

The computational fluid dynamics code CFD-ACE is being used in the current study to model and analyze the chemistry and heat and mass transfer for selected MOCVD reactors. The code is a three-dimensional control volume Navier-Stokes code with surface and gas phase chemistry. Several advanced features essential for modeling MOCVD systems have been incorporated into the code. These include models for non-gray radiation, Soret effects, multi-component diffusion, and advanced surface chemistry models using CHEMKIN.

3. RESULTS TO DATE

The numerical studies performed thus far can be placed in three categories: 1) thermal validation, 2) convection analysis, and 3) deposition predictions. These are discussed in more detail below.

Thermal Predictions

Thermal studies have been performed using data obtained by LaRC for pure gas flow in an MOCVD sled reactor. The apparatus used for these experiments is located in the Chemical Vapor Deposition Facility for Reactor Characterization at NASA Langley Research Center (Figure 1)¹. The reactor has a circular inlet section that feeds the reactants into a rectangular duct in which is mounted a fused silica sled containing a graphite susceptor. The graphite susceptor is heated by an external Radio Frequency (RF) induction coil (not shown in Figure 1), wound around the outside of the silica test section. The reactor was operated at various flow conditions using pure nitrogen, helium, and hydrogen (Table 1). During the experiment, the temperature along the sides and top wall of the reaction chamber was measured using an infrared camera². These data were subsequently used for model validation³.

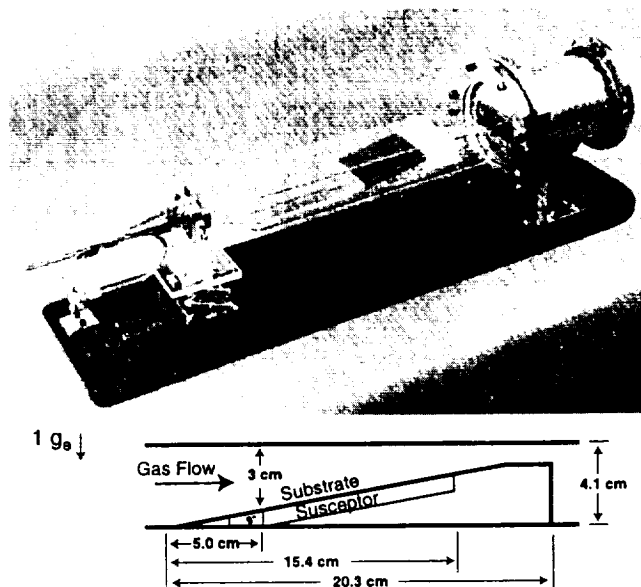


Figure 1. Experimental MOCVD Reactor at LaRC.

Table 1. Pure Gas Thermal/Flow Experiments Conducted at LaRC

$Gr/Re^2 = 27$	Hydrogen	Helium	Nitrogen
Flow Rate	9.9 lpm	N/A	9.9 lpm
Gr	200	N/A	9690
Re	2.7	N/A	18.9

$Gr/Re^2 = 41.5$	Hydrogen	Helium	Nitrogen
Flow Rate	8 lpm	8 lpm	8 lpm
Gr	200.0	171.0	9690
Re	2.2	2.0	15.3

$Gr/Re^2 = 166$	Hydrogen	Helium	Nitrogen
Flow Rate	4 lpm	4 lpm	4 lpm
Gr	200	171.0	9690
Re	1.1	1.0	7.6

$Gr/Re^2 = 664$	Hydrogen	Helium	Nitrogen
Flow Rate	N/A	N/A	2 lpm
Gr	N/A	N/A	9690
Re	N/A	N/A	3.8

$Gr/Re^2 = 2655$	Hydrogen	Helium	Nitrogen
Flow Rate	N/A	N/A	1 lpm
Gr	N/A	N/A	9690
Re	N/A	N/A	1.9

All the test cases in Table 1 were re-run using the numerical code. The model domain for these simulations consists of the entire reactor as shown in Figure 1, i.e., the chamber, the graphite susceptor,

the fused silica walls, and the fused silica susceptor holder. The gray radiation model assumption was used. The temperature on the reactor wall was determined as part of the solution, rather than specified a priori. The induction heating was modeled by fixing the graphite to 873K, as set in the experiment. The results of the simulation compare well with the thermal data³. For the range of Richardson numbers simulated, radiation and convection were both found to play significant roles in the heat transport in the reactor. Figure 2 shows a comparison of the empirical data with the numerical predictions for Nitrogen at $Ri = 41.5$ where Ri is the Richardson number, defined as Gr/Re^2 . (The “dips” in the experimental data are due to the RF coil obstructing the IR camera view). The agreement between the experimental data and the numerical model (e.g. to within 10 degrees for the wall temperature above the substrate) is considered to be satisfactory for first order simulations of the reactor environment. However, for very accurate analyses, additional physics, such as the non-gray radiation and the transient effects of surface emissivities need to be included. These mechanisms have been shown to be significant in commercial reactors and, as such, need to be precisely understood and modeled.

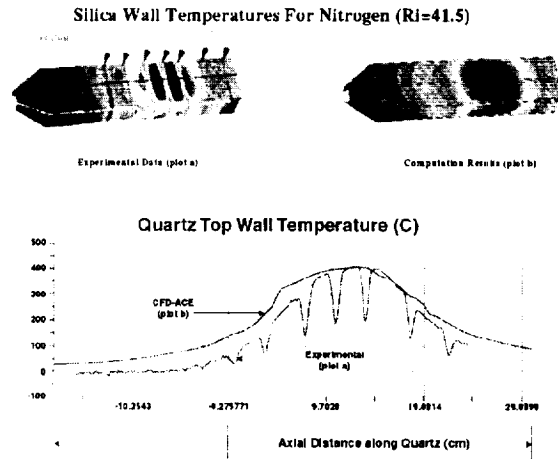


Figure 2. CFD-ACE: Thermal Prediction Validation for Nitrogen Flow in a CVD Reactor.

Flow Simulations

The parametric set of experimental test cases performed at LaRC were also analyzed numerically in terms of recirculation flows as a function of Richardson number. These parametric cases reconfirm the dependence of recirculation on the Richardson number and the existence of both longitudinal and transverse rolls for this reactor design⁵⁻⁹. Figure 3 show a comparison of the relative location and magnitude of the three dimensional recirculation zones inside the reactors as indicated by an iso-surface of reverse flow equal to one cm/sec. The results indicate the presence of recirculation. It was determined numerically that changing the reactor tilt could reduce the recirculation zones, however, since the simulations are for a non-reacting system, it is not possible to draw a correlation between the magnitude of the recirculation and the effect it would have on uniformity of deposition. This leads to the next phase of the study in which a reacting system is modeled.

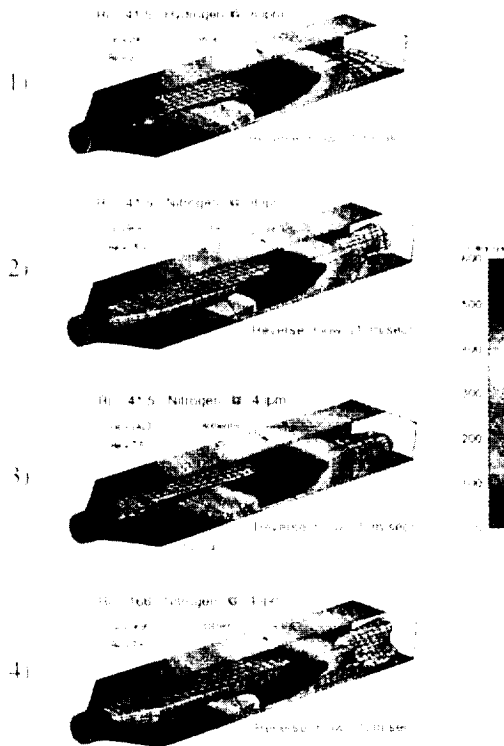


Figure 3. CFD-ACE: Recirculations Patterns for Pure Gases in an MOCVD as a Function of Ri #.

Reaction Simulation

The deposition of Indium Phosphide (InP) from the precursors Phosphine (PH₃), Trimethylindium (In(CH₃)₃), and Monomethylindium (InCH₃) was selected as the initial material for modeling. This system was selected because of the importance of InP as a semiconductor material and because of the availability of experimental data from the University of Virginia¹⁰. Furthermore, the data for this study were obtained using a commercial Crystal Specialties Model 425 MOCVD reactor (Figure 4) very similar in design to the test apparatus at LaRC.

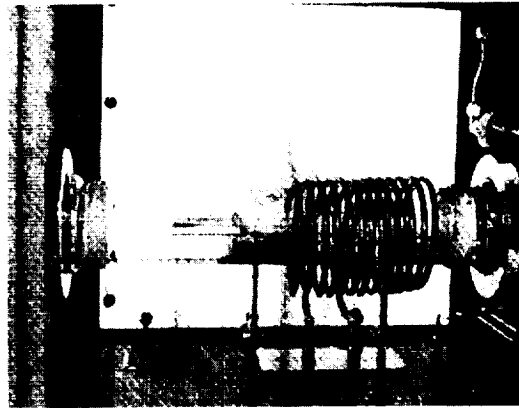


Figure 4. MOCVD Reactor at the University of Virginia.

The reaction set assumed for this system and the corresponding rate equations are shown in Tables 2 & 3 respectively¹⁰:

Table 2. Reaction Rates

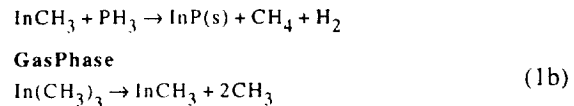
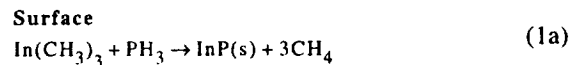


Table 3. Reaction Equations

$$\dot{\omega}_{\text{InP}} = \left\{ A_1[\text{TMI}]e^{-E_1/RT} + A_3[\text{MMI}]e^{-E_3/RT} \right\} \quad (2a)$$

$$\dot{\omega}_{\text{TMI}} = \left\{ -A_1[\text{TMI}]e^{-E_1/RT} - A_2[\text{TMI}]e^{-E_2/RT} \right\} \quad (2b)$$

$$\dot{\omega}_{\text{MMI}} = \left\{ A_2[\text{TMI}]e^{-E_2/RT} - A_3[\text{MMI}]e^{-E_3/RT} \right\} \quad (2c)$$

$$\dot{\omega}_{\text{PH}_3} = \left\{ -A_1[\text{TMI}]e^{-E_1/RT} - A_3[\text{MMI}]e^{-E_3/RT} \right\} \quad (2d)$$

$$\dot{\omega}_{\text{CH}_4} = \left\{ 3A_1[\text{TMI}]e^{-E_1/RT} + A_3[\text{MMI}]e^{-E_3/RT} \right\} \quad (2e)$$

$$\dot{\omega}_{\text{CH}_3} = \left\{ 2A_2[\text{TMI}]e^{-E_2/RT} \right\} \quad (2f)$$

$$\dot{\omega}_{\text{H}_2} = \left\{ A_3[\text{MMI}]e^{-E_3/RT} \right\} \quad (2g)$$

The activations energies for the reaction rates are based on the experimental measurements of Buchan, et al¹¹, and the pre-exponential factors were determined based on calibration with the empirical results¹⁰.

Table 4. Activation Energies

$$A_1 = 5 \times 10^5 \quad 1/\text{sec} \quad (3a)$$

$$A_2 = 1 \times 10^{14} \quad 1/\text{sec} \quad (3b)$$

$$A_3 = 1 \times 10^9 \quad 1/\text{sec} \quad (3c)$$

Table 5. Pre-exponential Coefficients

$$E_1 = 7.6 \times 10^7 \text{ J}/(\text{kgmol}) \quad (4a)$$

$$E_2 = 1.7 \times 10^8 \text{ J}/(\text{kgmol}) \quad (4b)$$

$$E_3 = 1.51 \times 10^8 \text{ J}/(\text{kgmol}) \quad (4c)$$

With the exception of the diffusivities, which are computed for each species based on kinetic theory, the physical properties of the mixture were assumed to be those of the predominate hydrogen. These properties were computed as follows¹⁰:

Table 6. Properties

Viscosity (kg / m - sec):

$$\mu = 2.907 \times 10^{-6} + 2.173 \times 10^{-8} \cdot T - 4.9167 \times 10^{-12} \cdot T^2 \quad (5a)$$

Specific Heat (J/kg - K):

$$C_p = 1.491 \times 10^4 - 1.644 \cdot T + 1.709 \times 10^{-3} \cdot T^2 \quad (5b)$$

Thermal Conductivity (W / m - K):

$$k = 9.6336 \times 10^{-3} + 3.453 \times 10^{-4} \cdot T - 1.413e-08 \cdot T^2 \quad (5c)$$

The run conditions used for the simulation are the same as UVA InP experimental run # 83 as listed below in Table 7.

Table 7. Run Conditions

Total Flow:

$$7720 \text{ sccm (cm}^3/\text{min)} \quad (1.1479 \text{ e-5 kg/s})^*$$

TMI (Trimethylindium) inlet concentration:

$$467\text{e-6 mole fraction (4.844e-4 mass fraction)}^{**}$$

TMI flow rate: 0.048 sccm

PH3 inlet concentration:

$$3.88\text{e-3 mole fraction (0.06179 mass fraction)}^{**}$$

PH3 flow rate: 30 sccm

Substrate temperature: 600°C (873 °K)

Pressure: 760 torr (1.013e4 nt/m³ or 1.0 atm)

* Based on a density of 0.0893 kg/m³ at T =

$$273^\circ\text{K and pressure} = 101300 \text{ nt/m}^2 \text{ (1 atm)}$$

** Based on a mixture molecular weight of 2.1349

The Reynolds Number ($Re = UL\rho/\mu$) for this simulation is 18. This is based on a length scale of 3 centimeters which is the channel height at the leading edge of the susceptor. The viscosity is 8.983e-6 kg/m-s, based on the inlet temperature (300K) and the viscosity formula in Table 6. The corresponding mixture density, at 1.0 atmosphere and 300 K, is 0.0862 kg/m³, as computed using the ideal gas law. The reference velocity, U, is .06255 m/s based on the above density, the cross-sectional area at the susceptor leading edge (2.743e-2 m²), and the mass flow rate (1.1479e-5 kg/s).

The Grashof Number ($Gr = g \beta [T_{\text{hot}} - T_{\text{cold}}] L^3/\nu^2$) for the simulation is 16.000. The T_{hot} is the substrate temperature of 873 °K and the T_{cold} is the inlet temperature of 300 °K. For an ideal gas, the thermal coefficient of expansion (β) is equal to $1/T$. For this case, β is approximated as a constant, $\beta = 1/T_{\text{ref}}$, where T_{ref} is set to the susceptor temperature (873/K). The length scale, L, and the kinematic viscosity $\nu = \mu/\rho$ (1.042 e-3 m²/s) are the same as

used for the Reynolds number and g is one earth's gravity.

The corresponding Richardson number (Gr/Re^2) is 49.

Simulation Results

Flow Pattern and Temperature Distribution:

Figure 5 shows the predicted flow pattern over the sled. At the Richardson number of 49, the flow pattern is dominated by forced convection, with minor recirculation zones above the leading edge of the substrate.

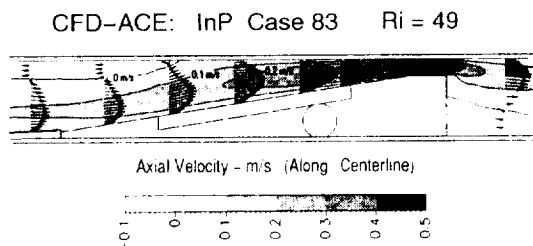


Figure 5. CFD-ACE Centerline Flow Pattern (Velocity Vectors) for UVA Case 83.

The corresponding centerline temperature contours are as shown in Figure 6.

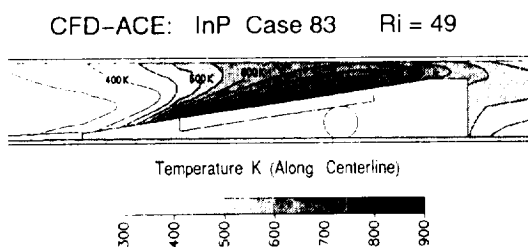


Figure 6. CFD-ACE Centerline Temperature Contours.

Predicted Deposition Rate: A full 3-D cut-away view (similar to the angle in Figure 1) of the model prediction is shown in Figure 7. The deposition rate of InP on top of the sled is indicated by the grey flooded surface contours and the x-y plot in the lower right-hand of the figure. The measured

deposition rate is included in the x-y plot as a dotted line. The deposition rate along the centerline exhibits a double peak near the leading edge of the substrate, as reported by Black¹⁰. This is caused by the dual surface deposition mechanisms (1a and 1b) listed in Table 2. Two-dimensional studies with a refined grid do a better job of reproducing the sharpness of these twin peaks. However, even grid refinement does not increase the average deposition rate predicted over the majority of substrate. In effect, the model is under predicting the deposition rate by nearly a factor of 2.

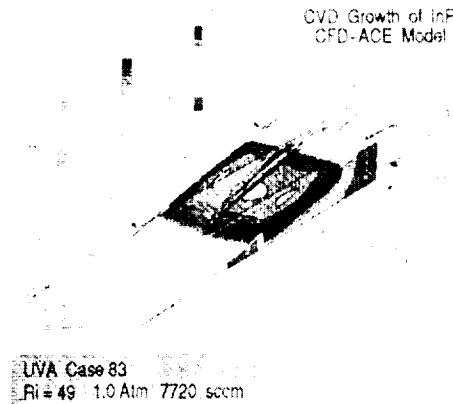


Figure 7. CFD-ACE Prediction Deposition Rates and Selected Surface Temperatures for InP at 7720 sccm at 1 atm ($Ri = 49$).

In an attempt to identify the cause of the discrepancy between the measured and predicted growth rates, several parametric studies were conducted to identify the sensitivity of the growth rate to the model assumptions. These include grid refinement, inlet swirl, modification of the pre-exponential coefficients (by 10%), gas radiative absorption, and substrate temperature (by 30 K). None of these were shown to increase the deposition rate significantly. This indicates that the predicted growth is diffusion limited. As shown by Figure 8, the concentration of MMI next to the substrate is severely depleted, thus limiting the growth rate. This was confirmed by increasing the reaction rate in Eq. 3c from 10^9 to 10^{20} with only a minor increase in the average growth rate.

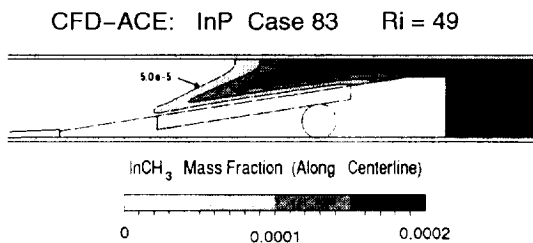


Figure 8. CFD-ACE Centerline Mass Fraction Contours.

The question therefore remains as to why the predicted growth rate of InP is less than the experimental rate. A very plausible explanation is provided by Black¹⁰ who points out that the InP growth in the experiments is polycrystalline and that in the initial stage of growth, it is relatively sparse, as shown in Figure 9. This is in contrast with the model which computes growth rates in terms of kg/m²-s and assumes a perfect surface. (Black's own simulation show a similar discrepancy between the experiments and predictions).

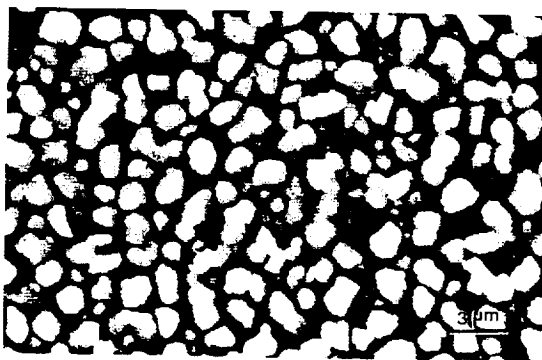


Figure 9. SEM micrograph of InP deposition on fused-silica after a growth time of 2 hours. Growth conditions the same as Run 32 (0.1 atm, 4420 sccm)¹⁰.

The above discrepancies point to the need for both better models and well controlled experiments. Towards that end, the current model will be extended to include more rigorous chemistry models with more complex gas phase chemistry and surface reactions including surface adsorbed species¹²⁻¹⁴

The material to be modeled with this advanced model will be the growth of GaAs, which is well characterized and for which there are high quality data available for comparison¹⁵⁻¹⁶.

4. SUMMARY/CONCLUSIONS

A full 3-D CFD model of a commercial MOCVD reactor has been developed and applied to model the growth of Indium Phosphide. The thermal predictive capability of the model has previously been validated using empirical data for pure gas flow. The model predictions for InP deposition, based on a simplified set of reaction equations are within a factor of two of the measured deposition. The empirical data itself is shown to be highly dependent on the polycrystalline structure and varies experimentally by a factor of two over a growth period of five hours. Parametric numerical studies indicates that the predicted growth rate is diffusion limited and relatively insensitive to grid refinement, increases with substrate temperature, inlet swirl, gas absorptivity, and variations in the pre-experimental factors.

The discrepancy between the predicted rate and the data is attributed to the polycrystalline nature of the growth surface and to the simplified chemistry mechanisms in the model.

The next phase of the project will study the deposition process with more complex (and realistic) chemistry models that account for surface adsorbed species. Once these improvements have been sufficiently validated, the model will then be used to better understand the combined role of radiation/convection on the MOCVD deposition process.

ACKNOWLEDGEMENTS

The authors would like to express appreciation to Professor William A. Jesser and Mr. Will Clements of the Materials Science and Engineering Department of the University of Virginia for providing data and valuable discussions on the UVA studies. This work was performed for NASA under contract NAS8-40846.

REFERENCES

- 1) E.J. Johnson, P.V. Hyer, P.W. Culotta, L.R. Black, I.O. Clark and M.L. Timmons (1991), "Characterization of MOCVD Fluid Dynamics by Laser Velocimetry," *J. Crystal Growth*, Vol. 109, pp. 24-30.
 - 2) P.V. Hyer (1997), Use of Infrared Imagery in Characterization of Chemical Vapor Deposition Reactors," *Infrared Physics & Tech* 38, pp. 17-24.
 - 3) M. Kannapel, S.A. Lowry, A. Krishnan, I.O. Clark, P. Hyer and E. Johnson (1997), "Preliminary Study of the Influence of Grashof and Reynolds Numbers on the Flow and Heat Transfer in an MOCVD Reactor," *APIE Annual Conference*, July 28-29, San Diego, CA, Vol. 3123.
 - 4) F. Durst, L. Kadinski, Yu.N. Makarov, M. Schafer, M.G. Vasil'ev, and V.S. Yuferev (1997), "Advanced Mathematical Models for Simulation of Radiative Heat Transfer in CVD Reactors," *J. Crystal Growth*, Vol. 172, pp. 389-395.
 - 5) A.B. Bulsar, M.E. Orazem, and J.G. Rice (1988), "The Influence of Axial Diffusion on Convective Heat and Mass Transfer in a Horizontal CVD Reactor," *J. Crystal Growth*, Vol. 92, pp. 294-310.
 - 6) J. Ouazzani and F. Rosenberger (1990), "Three-Dimensional Modeling of Horizontal Chemical Vapor Deposition I. MOCVD at atmospheric pressure," *J. Crystal Growth*, Vol. 100, pp. 545-576.
 - 7) D.I. Fotiadis, M. Boekholt, K.F. Jensen, and W. Richter (1990), "Flow and Heat Transfer in CVD Reactors: Comparison of Raman Temperature Measurements and Finite Element Model Predictions," *J. Crystal Growth*, Vol. 100, pp. 577-599.
 - 8) E.P. Visser, C.R. Kleijn, C.A.M. Govers, C.J. Hoogendoorn, and L.J. Giling (1989), "Return Flows in Horizontal MOCVD Reactors Studied with the Use of TiO₂ Particle Injection and Numerical Calculations," *J. Crystal Growth*, Vol. 93, pp. 929-946.
 - 9) P.B. Chinoy and S.K. Ghandhi (1991), "Design Considerations for the Elimination of Recirculation in Horizontal Epitaxial Reactors," *J. Crystal Growth*, Vol. 108, pp. 105-113.
 - 10) L.R. Black (1993), "Three-Dimensional Numerical Modeling of InP MOCVD with Experimental Verification," Dissertation, University of Virginia, Department of Material Sciences and Engineering.
 - 11) N.I. Buchan, C.A. Larsen, and G.B. Stringfellow (1988), "A Mass Spectrometric Study of the Simultaneous Reaction Mechanism of TMIn and PH₃ to Grow InP," *J. Crystal Growth*, Vol. 92, pp. 605-615.
 - 12) K.F. Jensen, D.I. Fotiadis, and T.J. Mountziaris (1991), "Detailed Models of the MOVPE Process," *J. Crystal Growth*, Vol. 107, pp. 1-11.
 - 13) M. Tirtowidjojo and R. Pollard (1988), "Elementary Processes and Rate-Limiting Factors in MOVPE of GaAs," *J. Crystal Growth*, Vol. 93, pp. 108-114.
 - 14) M. Tirtowidjojo and R. Pollard (1989), "The Influence of Reactor Pressure on Rate-Limiting Factors and Reaction Pathways in MOVPE of GaAs," *J. Crystal Growth*, Vol. 98, pp. 420-438.
 - 15) T. Bergunde, F. Durst, L. Kadinski, Yu.N. Makarov, M. Schafer, and M. Weyers (1994), "Modeling of Growth in a 5 x 3 Inch Multiwafer Metalorganic Vapour Phase Epitaxy Reactor," *J. Crystal Growth*, Vol. 145, pp. 630-635.
 - 16) A.P. Peskin and G.R. Hardin (1998), "Gallium Arsenide Growth in a Pancake MOCVD Reactor," *J. Crystal Growth*, Vol. 186, pp.494-510.
 - 17) T. Bergunde, J. Dauelsberg, L. Kadinski, Yu.N. Makarov, M. Weyers, D. Schmitz, G. Strauch, and J. Jurgensen (1997), "Heat Transfer and Mass Transport in a Multiwafer MOVPE Reactor: Modeling and Experimental Studies," *J. Crystal Growth*, Vol. 170, pp. 66-71.
- A CFD Research Corporation, 215 Wynn Dr., Huntsville, AL 35805; sal@cfdr.com; (256) 726-4853
 B CFD Research Corporation, 215 Wynn Dr., Huntsville, AL 35805; ak@cfdr.com; (256)726-4816
 C NASA Langley Research Center, MS 473, Hampton, VA 23681

